IAC-20-C1.6.10

Modelling the break-up and re-entry propagation of meteorites through a continuum approach

Limonta S.[a]*, Trisolini M.[b], Frey S.[c], Colombo C.[d]

[a ,b ,c ,d] *Politecnico di Milano, Department of Aerospace Science and Technologies, Via La Masa 34, 20156 Milano*
[a] simone.limonta@mail.polimi.it
[b] mirko.trisolini@polimi.it
[c] stefan.frey@polimi.it
[d] camilla.colombo@polimi.it

* Corresponding Author

Abstract

The study of the fragmentation of meteorites entering the Earth's atmosphere allow to predict the consequences such events can have on the ground. Existing models for meteoroid fragmentation follow either a pancake approach, where the cloud of fragments resulting from the meteorite explosion expands together in the shape of a disk, or a discrete fragmentation approach, where successive fragmentation events split the bolide into several pieces. In this work, a comprehensive approach in which the fragments resulting from the breakup of a meteorite are modelled using a continuum distribution it is proposed. A modified version of the NASA Standard Breakup Model is used to generate the fragments distribution in terms of their area-to-mass ratio and ejection velocity. This distribution is then combined with the nominal entry state of the meteorite to generate the initial conditions for the entire ensemble of fragments resulting from the breakup. The fragments distribution is then directly propagated using the continuity equation combined with the non-linear entry dynamics, considering both deceleration and ablation. The result is the evolution of the fragments cloud in time, which is then reconstructed at each time step using a Gaussian mixture model. This model moves away from the simplified pancake method and has the flexibility to include large fragmentation events for a better physical representation of the entry of meteorites, given the fragments distribution as an initial condition only. This means that improved meteorites fragmentation models can be easily integrated into this framework for better propagation of the trajectory of the fragments. The propagation of the fragments density and its reconstruction is first compared against Monte Carlo simulations, and then against real observations.

Keywords: Asteroids, Meteoroid, Asteroid entry, Asteroid fragmentation, Strewn field, Ground footprint

Nomenclature

L_c	Characteristic length
N_c	Number of fragments generated bigger than a given L_c
N_{tot}	Total number of fragments
c_d	Drag coefficient
$p_{a,b}$	Probability density function in a,b space
ρ_m	Meteoroid density
σ_{ab}	Ablation coefficient
h	Altitude
A/M	Area-to-mass ratio
M	Meteoroid mass
R	Meteoroid radius
S	Meteoroid strength limit
f	Power factor of the L_c distribution
k	Tuning parameter for mass conservation
n	State space density
v	Velocity
w	Bin relative weight
$\mathcal{N}$	Normal distribution
γ	Flight path angle
δ	Latitude
ζ	Angular range
λ	Longitude
ρ	Air density

Acronyms/Abbreviations

ABM	Asteroid Breakup Model
CDF	Cumulative Density Function
GMM	Gaussian Mixture Model
PDF	Probability Density Function
SBM	Standard Breakup Model

1. Introduction

Every day roughly 70 000 000 meteoroids enter the Earth's atmosphere. While the vast majority are small and burn up harmlessly during the descent, more than 1000 kg per day of meteoroid material reaches the surface of the Earth, accounting for about 1% of the total meteoroids mass [1].

In 2013 the Chelyabinsk event [2] motivated new assessments of the potential risk posed by mid-sized asteroids that may not be large enough to cause cratering or global-scale effects, but may still produce significant ground damage. To enable the assessment of these risks, models of asteroid entry and fragmentations are needed, together with accurate post breakup trajectory

simulations. Existing models for meteoroid fragmentation follow either continuum [3] or discrete [4–8] approaches. Recently also models that derive from a combination of both have been proposed [9,10]. These models are often useful for approximating the fragmentation process and the resulting deposition of kinetic energy in the atmosphere, but they tend to lack a detailed treatment of the breakup and of the interactions between individual fragments.
For this reason, in the interest of developing a physically consistent fragmentation model suitable for probabilistic analysis, the current work introduces a continuous, semi-analytical approach for modelling fragmentation events, derived from a modified version of the NASA Standard Breakup Model (SBM). Then, a density-based methodology is applied to the cloud of fragments generated for evaluating the meteorites strewn field as alternative to the traditional Monte Carlo method.

Several models describing the fragmentation of meteoroids under the action of aerodynamic forces can be found in literature. Depending on the approach used, they can be split in two classes: semi-analytical models (continuous, discrete or hybrid) and hydrodynamics models. Hydrocode simulations consider the object in quasi-liquid state evolving in a hypersonic flow. They can capture the detailed flow physics and material properties; however, they are not suitable for running the many cases needed for a probabilistic approach to risk assessment. Some address interactions between fragments, but are constrained to specific configurations [11] or with limited number of fragments [6].

On the contrary, semi-analytic breakup models permit probabilistic studies using assumptions that simplify the problem. They are typically based on the single-body meteor physics equations [12] and the fragmentation events are assumed to occur when the dynamic pressure at the stagnation point of a bolide exceeds its yield strength [1,7]. The fragmentation products are typically represented either as a cloud-like structure, a number of discrete fragments, or some combination of both.

The most basic example of continuous model is the so called “pancake model” [3]. At the breakup point, the meteoroid becomes a cloud of continuously fragmenting material. The cloud starts as a sphere and behaves as a single deforming body. During the descent it begins to spread out and flatten due to pressure differences between the front and sides of the debris cloud. While the body is expanding the void, that should form between the small fragments, is instead occupied by other debris continuously created by the fragmentation. This model provides a good description of the energy deposition but does not allow for variations that could result from non-uniform asteroid structures and the behaviour of large, independent fragments.

Examples of discrete fragmentation models are given by the “collective wake model” [5] and “non collective wake model” [13]. They both assumes that at the breakup the meteoroid divides in two identical child-fragments whose strength depends on the parent asteroid strength by means of a Weibull scaling law [14]. After a few steps, a cloud of identical fragments is produced. The two models differentiate themselves in how the fragments interacts with each other. In the first case, they fly side by side and proceed under the same bow shock increasing the total frontal area and conserving the original object’s mass. In the second case one of the child-fragments is simply lost to the wake, so that at each fragmentation the area is preserved, and the mass is halved. The assumption of two even fragments resulting from each break is a strong assumption of the breakup process, but it could represent the average rate of fragmentation. It should be noted some geometric inconsistencies in the “collective wake model” scheme, as spheres consisting of half the original mass will not double the drag area [10].

A more general discrete model, the “independent wake model” [7], consider the two fragments generated at each breakup step to behave independently from each other and assign to each of them a lateral spread velocity. The main disadvantage of this scheme it does not consider that multiple fragmentations at the same time. Moreover, it is assumed that the fragments produced at each breakup will be stronger than the parent fragment, because the breakup would eliminate some of the larger structural weaknesses. However, this is not a general rule: a piece of meteoroid could also develop new fractures that could reduce a lot its new strength.

The most recent example of hybrid model combines the features of the “independent wake model” and the “pancake model” to capture both continuous and discrete variation of the kinetic energy of the meteoroids [9,10]. At the breakup the bolide is assumed to break into three objects: two spherical fragments and a dust cloud. The cloud is modelled as a continuum using the pancake approximation. At the same time, the two child-fragments continue their descent independently until a new fragmentation point is reached, then for each fragment two new child-fragments and a new dust cloud are formed. This model can reproduce observed light curves well, but also maintains the criticalities of the pancake approach when modelling the smaller fragments. Regarding the discrete part, it has the strong limitation of considering all the fragments velocity unchanged with respect to the original body and does not consider a side velocity component so that cannot be used form for any three-dimensional analysis.

The “sandbag model” [6] is an example of semi analytical model built starting from the results obtained using detailed hydrodynamics simulation. The deforming meteoroid is represented as a cone rather than a sphere by including both streamwise and spanwise separation. The

main disadvantage of the presented model, accordingly to the author, is a strong deficiency of very small fragments (much smaller than the largest one).
Lastly, the "multi-component fragment cloud model" [15] assumes that the asteroid has a non-uniform internal structure. The initial body is constructed as a multi-component object comprising different structural groups with different initial strengths. The most fragile components will break off and begin fragmenting at the highest altitude, while the most resilient components will start to breakup close to the surface. The main criticality of this model is the arbitrariness of the initial composition of the body and the intrinsically discretised nature of the debris cloud: for each group of strength, all the fragments parameters are identical to each other.

The present work shows the development of a novel methodology for the assessment of asteroids re-entry, fragmentation, and impact. This analysis aims at modelling the small asteroids and large meteoroids, hence excluding the rubble pile asteroid. The work proposes a novel, continuous, Asteroid Breakup Model (ABM) that provides a statistical description of the fragments generated, in terms of velocity, flight path angle, and area-to-mass ratio. Then, is proposed a methodology that implement a density-based method, alternative to the traditional Monte Carlo approach, for the estimation of the fragment's evolution during the descent. In this work, this methodology has been used for the identification of the on-ground footprint of the fragments.

2. Asteroid breakup model

Accordingly to Ceplecha [16], during the atmospheric entry the asteroids can fragments in one or multiple points along their trajectory: in the first case the asteroid is typically destructed in many small fragments, while in the second case at each fragmentation point the meteoroid breaks approximately in two halves together with dust and smaller fragments.

The fragmentation model developed here aims to be an exhaustive and complete description of the distribution of the fragments cloud generated by the bolide disruption. Considering that the meteoroid atmospheric fragmentation is a rare observed phenomenon, the baseline used as reference in this analysis is searched looking at similar phenomena, namely, in space debris field.

Indeed, spacecraft re-entry and upper stages explosion have been considered suitable for this purpose and the NASA SBM traditionally used for modelling fragmentation in orbit (not during re-entry) has been considered appropriate to this purpose. This is also is strengthened from the fact that the NASA SBM has already been used for re-entry analysis in the debris field, for example it is implemented in the Debris Risk Assessment and Mitigation Analysis (DRAMA) suite [17,18].

2.1 NASA Standard Breakup Model

The NASA Standard Breakup Model is a commonly used empirical model that describes the outcome of satellites fragmentations. The model describes the fragments generated from an explosion or collision in terms of number, size and area-to-mass ratio distributions. In addition, it defines a fragments ejection velocity distribution with respect to the parent object.

The equations of the NASA SBM model can fully characterise a debris cloud, but, as highlighted by Krisko [19], the applicability of the breakup model is set between 1mm to meter sized fragments and it does not guarantee the total mass of the parent body. Therefore, corrections are required to fully adapt the model to the modelling of an asteroid breakup event. In the following paragraphs the distributions used for building the ABM is described and discussed.

2.2 Characteristic length distribution

The empirical characteristic length distribution of the fragments suggested by the NASA SBM is a power law distribution with the following expression:

$$N_c = k\, L_c^{-f} \tag{1}$$

where N_c is the number or fragments generated bigger than a given characteristic length L_c, f is a fixed scale factor ($f = 1.6$) and k is a tuning parameter that depends on the object that undergoes fragmentation [20].

In many cases in nature, fragmentation results in a fractal distribution: fragments produced by explosions and impacts often shows this behaviour that can be mathematically represented by means of a power law, as in the NASA SBM (1) [21]. This support the idea of extending this distribution also including the characterisation of asteroids breakup. The validity of such an extension is also supported by the analysis of the meteorites collected on the ground after entry events characterised by intense fragmentation. Although, these findings are biased from the ablation process and from the multiple fragmentations, the number of fragments in relation on their mass follows approximately a power low [22,23].

Starting from the cumulative distribution of Eq. (1), the characteristic length probability distribution is obtained firstly expressing it as the standard Cumulative Distribution Function (CDF).

$$CDF_L = \frac{N_{tot} - N_c}{N_{tot}} \tag{2}$$

where N_{tot} represents the total number of fragments produced at the breakup, which is given by

$$N_{tot} = k\left(L_{min}^{-f} - L_{max}^{-f}\right) = k\,\alpha \tag{3}$$

and L_{min} and L_{max} are the maximum and minimum characteristic length of the fragments generated at the breakup, respectively. At this point the characteristic length probability density function can be expressed by taking the derivative of the CDF_L with respect to L_c as follows:

$$p_L = \frac{dCDF_L}{dL_c} = \frac{f}{\alpha}\,L_c^{-f-1} \tag{4}$$

2.3 Area-to-Mass distribution

In the NASA SBM, the A/M distribution assumes that the fragments generated at breakup have different density values. This assumption is reasonable for spacecrafts or rocket bodies because they are composed of different materials, but it is not valid for meteoroid. In this analysis, they are assumed to have uniform density; for this reason, the original A/M distribution must be modified. To conserve the density value, the fragments are assumed to have a spherical shape. While this can seem a strong assumption, this is a common choice in most of the models used in literature. In fact, the shapes of asteroids are typically irregular and not well known before the impact. Moreover, they are modified by ablation during entry. The spherical shape approximation is therefore considered a suitable compromise between model simplicity and accuracy.

Using this approximation, the characteristic length can be defined as the object diameter; therefore, the relations between the geometrical parameters can be expressed as follows:

$$L_c = 2\,R \tag{5}$$

$$A/M = \frac{3}{2\,\rho_m\,L_c} \tag{6}$$

$$M = \left(\frac{3}{4\,\rho_m}\right)^2 \frac{\pi}{(A/M)^3} \tag{7}$$

where ρ_m is the meteoroid density and M is the meteoroid mass.

By means of Eq. (5), together with Appendix A, it is possible to obtain an alternative expression for p_L expressed in terms of A/M. The PDF distribution obtained is the following:

$$p_{A/M} = \frac{f}{\alpha}\,(2/3\,\rho_m)^f\,A/M^{f-1} \tag{8}$$

It represents the number of fragments (normalised) having a selected A/M.

2.4 Mass conservation

In literature a univocal method is not prescribed to implement the mass conservation in the NASA SBM [19]. For example, it is possible to use scheme based on iterative computations, suitable for a Monte Carlo approach [24] but for the purpose of this work a distribution function that guarantee the mass conversion is required. The power law distribution of Eq. (1) has a free parameter k that can be tuned depending on the object that undergoes the fragmentation process. It is possible to rewrite the probability density function in terms of the fragments mass (9) without changing the area underlying the function, following the transformation methodology presented in Appendix A (Probability density function transformation)

$$p_M = \frac{f}{3\alpha}\left(\frac{\pi}{6}\,\rho_m\right)^{f/3} M^{-f/3-1} \tag{9}$$

p_M is the result of a coordinate transformation, hence it still represents, the frequency of a fragment of a given mass (i.e. p_M represents the normalised number of fragments having the same mass M_i), therefore:

$$\int_{M_{min}}^{M_{max}} p_M\,dM = 1 \tag{10}$$

and

$$\int_{M_{min}}^{M_{max}} p_M\,N_{tot}\,dM = N_{tot} \tag{11}$$

To obtain the normalised mass of the fragments it is sufficient to multiply p_M (i.e. the normalised number of fragments) by M, as in Eq. (10). The total mass is found by multiplying the result times the total number of fragments, N_{tot} as shown in Eq. (11). The parameter k is then found by imposing the mass conservation as follows:

$$N_{tot}\int_{M_{min}}^{M_{max}} M\,p_M\,dM = M_{tot} \tag{12}$$

Whose solution is:

$$k = \frac{M_{tot}}{\frac{f}{3-f}\left(\frac{\pi}{6}\,\rho_m\right)^{f/3}\left(M_{max}^{1-f/3} - M_{min}^{1-f/3}\right)} \tag{13}$$

The Eq.(13) shows that the parameter k can be determined only by imposing the mass range of the fragments generated. This condition is traduced in a boundary definition of the minimum and maximum characteristic length in the fragments cloud. However, there is not a fixed rule for choosing them, they must be selected depending on the specific event analysed.

2.5 Velocity distribution

In the NASA SBM, the velocity distribution is modelled as a log-normal PDF as follows:

$$p_{v|\chi} = \mathcal{N}(\mu, \sigma) \tag{14}$$

where:

$$\sigma = 0.4$$
$$\mu = 0.2\,\chi + 1.85$$
$$\chi = Log(A/M)$$
$$\nu = Log\ (\Delta v)$$

However, this model expresses only the magnitude of the velocity variation, not its direction. A model of the ejection directions is then required to properly describe a breakup. Looking at the observations there is no evidence of a preferred ejection direction during fragmentations, so the impulse direction is assumed to be uniformly distributed. To introduce a directional component in the probability density functions of Δv, the distribution needs to be divided by the surface area that the tip of the velocity vector draws out [25].

$$p_{\Delta v} = \frac{p_{\Delta v}}{\mathcal{S}} \tag{15}$$

$$\mathcal{S} = \begin{cases} 2\,\pi\,\Delta v & for\ planar\ case \\ 4\,\pi\,\Delta v^2 & for\ spherical\ case \end{cases} \tag{16}$$

2.6 Joint-PDF

As outlined in the introduction, this new model produces a joint probability density function in the phase space of the problem. The selected states are the parameters that better characterise the fragment behaviour in the cloud: area-to-mass ratio (A/M), velocity (v) and flight path angle (γ). The procedure outlined in this paper is specified for the planar case (three-state model) to allow for a clearer description of the model; however, the ABM can be readily extended to a three-dimensional case (six-state model).

Before merging the two distributions and obtaining the joint PDF, the variables must be changed. Using the relation in Appendix A (Probability density function transformation).

$$p_\chi = ln(10)\ 10^\chi\ p_{A/M} \tag{17}$$

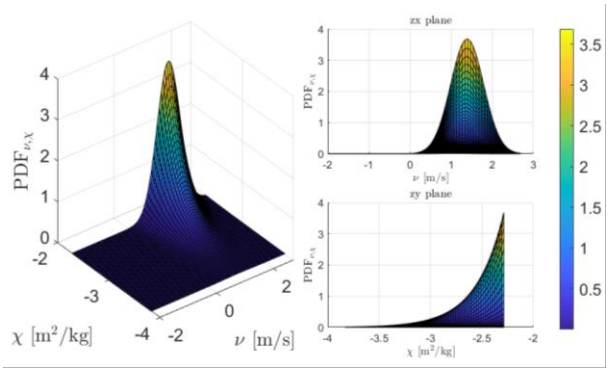

Fig. 1. Probability density function of ν, χ. This distribution is relative to the asteroid breakup analysed in Sec. 5

At this point the PDF in the χ, ν space is obtained by multiplying the probability density functions (Fig. 1):

$$p_{\nu,\chi} = p_{\nu|\chi}\ p_\chi \tag{18}$$

Then the usual relation is used to transform the PDF back to the original variables (Fig. 2):

$$p_{A/M,\Delta v} = p_{\nu,\chi}\ \frac{1}{ln^2(10) A/M\ \Delta v} \tag{19}$$

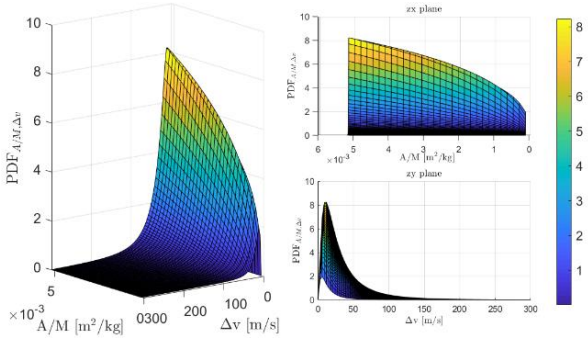

Fig. 2. Probability density function of $A/M, \Delta v$. This distribution is relative to the asteroid breakup analysed in Sec. 5

At the end the joint PDF is obtained by adding the direction dependence of the impulse as explained in Sec.2.5.

$$p_{A/M,v_x,v_y} = p_{A/M,\Delta v}\ \frac{1}{\mathcal{S}_{2D}} \tag{20}$$

The joint probability density function is now function of $A/M, v_x, v_y$ where v_x and v_y are the Δv component along the trajectory and normal to it at the breakup point respectively. One more transformation is required to move the function in the chosen state space, obtaining the final expression of the joint PDF (Fig. 3):

$$p_{A/M,v,\gamma} = p_{A/M,v_x,v_y}\ |v| \tag{21}$$

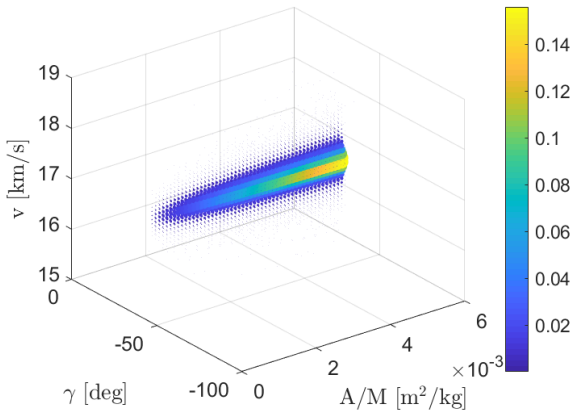

Fig. 3. Joint PDF in the phase space. The colour and the size of the dots indicates the value of the probability at

each point. The distribution is relative to the asteroid breakup analysed in Sec. 5.

3. Density based approach

The ABM describes the fragments cloud as a whole, by means of a joint PDF. Its intrinsic continuous nature allows to exploit a new strategy, alternative to the Monte Carlo method, for the propagation of the fragments dynamics.

This methodology, presented for the first time by Heard [26], is based on a continuous approach. The coupling between the dynamics and the continuity equation enables the exact evaluation of the evolution in time of the joint PDF. The central idea of this approach is to consider the fragments population as a fluid with continuous properties. In this way, the analysis of the single objects is abandoned, and the ensemble of fragments together with their density is considered. Once the initial distribution of the fragments is known, the continuity equation (22) is used to obtain its evolution in time.

$$\frac{\partial n}{\partial t} + \nabla \cdot \boldsymbol{f} = n^+ - n^- \tag{22}$$

Where n represents the fragments density in the space of the entry coordinates and the vector field $\boldsymbol{f}$ describe the differential problem. The divergence of $\boldsymbol{f}$ accounts for continuous phenomena (e.g. drag, ablation) and n^+, n^- are respectively the source and sink terms that model discontinuous events.

This method is quite general and it has also been applied to describe the evolution of interplanetary dust [26], nano-satellites constellations [27] and debris cloud evolution [28,29]. Trisolini [30,31] and Halder [32] recently applied this approach to the re-entry of satellite debris. The present work aims to improve this model by introducing the physics related to ablation and fragmentation.

3.1 *Dynamics*

Most of the dynamic models used in meteor science are based on a two-dimensional motion. This simplification can be justified observing the shape of the meteoroids foot-print: typically the fragments distribute across an elongated elliptic area, called strewn filed [33]. The major axis of the ellipse coincides with the direction of motion of the meteorite swarm and for a preliminary analysis can be approximated as a line.

Following the procedure outlined by Register [10], it is assumed a planar reference frame over a circular, non-rotating, Earth (Fig. 4). The meteoroid is modelled as a point mass with uniform density and area-to-mass ratio, subject to Earth gravity, air resistance and ablation. Lift forces, accordingly to the most recent models in literature [7,10], are not considered, in fact meteoroids are, in general, heavy and non-aerodynamic bodies. Moreover, the unknown shape of these objects does not allow to determine a reliable value for the lift coefficient.

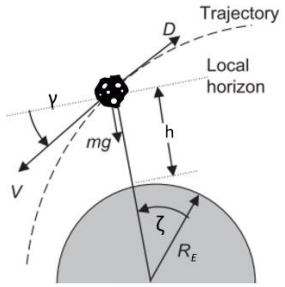

Fig. 4. Planar reference system

The meteoroid entering the Earth's atmosphere is governed by a modified version of the of the single body set of equations [34], proposed by Register et al. [10]. At this point, the continuity equation can be added to this set, and after exploiting the method of the characteristic [27, 30,32], the system can be written in the phase space of the dynamic:

$$\begin{cases} \dot{h} = v\ sin\gamma \\ \dot{\zeta} = \dfrac{v\ cos\gamma}{R_E + h} \\ \dot{v} = \dfrac{\rho\ v^2 A/M\ c_d}{2} - g\ sin\gamma \\ \dot{\gamma} = cos\gamma\ \left(\dfrac{v}{R_E + h} - \dfrac{g}{v}\right) \\ \dot{A/M} = \dfrac{1}{6}\ \rho\ c_d\ \sigma_{ab}\ (A/M)^2\ v^3 \\ \dot{n} = \left[sin\gamma\left(\dfrac{v}{R_E + h} - \dfrac{g}{v}\right) + \rho\ vA/Mc_d + \cdots \right. \\ \qquad \left. \cdots - \dfrac{1}{3}\ \rho\ c_d\ \sigma_{ab}\ A/M\ v^3\right]\ n \end{cases} \tag{23}$$

where h is the altitude from the ground, v is the fragment velocity and γ is the flight path angle. The gravity acceleration (g) is modeled as a function of the altitude by means of an inverse square model, while for the atmospheric density (ρ) an exponential model has been adopted. The drag coefficient (c_d), can be considered constant at high hypersonic regime, since it is independent on the Mach number. For the case in exam is considered $c_d = 1$ as reference value [10]. σ_{ab} is the ablation coefficient, as pointed out by Wheeler [9], the ablation rate should vary with fragment size, shape, speed, and altitude throughout entry. However, appropriate values for those rates and how much they may vary throughout entry remain uncertain. In this analysis is selected the baseline value of $\sigma_{ab} = 10^{-8}\ s^2 m^{-2}$ adopted both from Register [10] and Hills [3], that is defined for the evolution of a fragments cloud. ζ is a generic angular variable representing the angular range distance from the atmospheric entry. The ground

distance covered by the flying object is called range, it can be found by multiplying ζ times the Earth radius.

3.2 Augmented PDF

In the formulation of the problem previously described, the density function is referred only to the fragment cloud distribution. However, it should be noted that the versatility of the density-based method allows to easily modify the density function. In particular, also the uncertainties can be modelled as density function. The approach presented does not distinguish between the two types of densities, in this way it is possible to augment the three-dimensional joint PDF (A/M, v, γ) with any source of uncertainties. During the meteoroid entry, the main uncertainty source, is considered to be the estimation of the position of the meteoroid in the sky. It is also difficult to predict when, along the trajectory the fragments generated stop to influence each-other. This time uncertainty can be considered also as a position uncertainty of the meteoroid at the breakup. The position uncertainty is traduced in two independent uncertainties: range and altitude. The uncertainties distributions are considered as Gaussian normal distribution and are assumed independent from all the other states. Following this procedure, the joint PDF is transformed in a 5-dimension function, accordingly to the set of the dynamic equation, and it can be expressed as follow:

$$p_{augmented} = p_{A/M,v,\gamma}\, p_h\, p_{range} \tag{24}$$

where p_h and p_{range} are defined as Gaussian uncertainties having a 10% relative variance.

3.3 Fitting and marginalisation

The density-based propagation performed through the method of characteristics results in a discrete set of samples carrying the information on the actual fragment density for the defined phase space. To obtain the density information in the entire domain, the distribution has to be reconstructed at each integration step by interpolating the scattered data over the phase space domain. In the present work, the density distribution is reconstructed by fitting it to a Gaussian Mixture Model (GMM).

This method has been proposed by Frey et al. [35] for the reconstruction of the fragments density following a catastrophic fragmentation of a satellite in orbit. The GMM is fit using a gradient descent optimization method to minimize a given cost function dependent on the densities of each sample. This procedure is automatically implemented by the Starling suite, a novel tool developed at the Politecnico di Milano and funded by the COMPASS European Research Council project and the European Space Agency [28]. The suite has been designed to estimate evolving continua subject to non-linear dynamics and consists of several independent routines. In this paper, the fitting routine has been exploited, with minor changes in order to adapt it to the meteoroid entry dynamics. Further details about the Starling suite and its fitting optimisation technique can be found in Frey et al. [28,35].

It should be noted, however, that during the propagation both the density and the volume of the phase space deform. It is possible that the domain shape increases its complexity over time. In these cases, the fitting routine might provide inaccurate results.

Once the joint PDF has been evaluated, it is possible to compute its marginal along each dimension (i.e. the probability of an event irrespective of the outcome of other variables). For example, the one-dimensional marginal probability along the x-direction of a three-dimensional distribution function $p(x, y, z)$ is expressed by:

$$m_x = \iint p(x, y, z)\, dy\, dz \tag{25}$$

In this framework, the marginalisation of the multivariate normal distribution over one or more distributions is another multivariate normal distribution. The new mean and covariance are simply the partitioned mean and covariance of the marginalised distribution. The extension to the marginalisation of a GMM is trivial.

3.4 *Three-dimensional extension*

Analyzing the meteoroid entry, it is possible to extend the results of the planar dynamic model (Sec. 3.1) to describe a full three-dimensional motion.

Considering the three-dimensional set of equations governing the descent of a non-lifting object in the atmosphere for a non-rotating Earth [36], the main difference with Eq. (23) is the presence of the heading angle (χ) defined as the angle between the local meridian and the projection of the velocity vector on the local horizon and of the latitude (δ) and longitude (λ) instead of the angular range (ζ). As pointed out by Avanzini [36] for a motion constrained over any plane containing a great circle the equations of motion reduce to the two-dimensional set of Eq. (23). For this reason, the meteoroid entry can be modelled using the two-dimensional equations until the breakup. This approximation, in general, it is not valid when propagating the fragments cloud after the breakup. During fragmentation, in fact, in a three-dimensional analysis, the velocity is scattered also in the out-of-plane direction.

In this case, the heading angle χ is added as new state in the joint PDF. However, the heading angle variation, during the fragments descent, can be neglected at small latitude angles without generate large errors. Following these considerations, χ can be approximated constant and this allows to decouple the heading angle from the other equations. The only remaining variables that depend on χ at this point are the latitude δ and the longitude λ, as χ is

assumed constant in time and that δ is small (i.e. cos δ ~ 1) they can be considered as the projection of the angular range (ζ) in two orthogonal direction (North and East).

The three-dimensional dynamics reduces to the usual two-dimensional dynamics, with the inclusion, ex-post, of the χ dependence, used to decompose the angular range in latitude and longitude. In a similar way, considering χ constant, its initial distribution is not changing through the descent: to recover the three-dimensional joint PDF it is sufficient to multiply the distribution associated with the two-dimensional dynamics with the χ distribution, because they are independent.

$$p_{A/M,v,\gamma,\chi,h,r} = p_{A/M,v,\gamma,h,r}\ p_{\chi} \tag{26}$$

4. Model application

In this analysis, the focus has been on the meteoroid ground footprint determination and on the fragments distribution inside this region. These variables are indeed two of the most relevant in a risk assessment analysis. However, by exploiting this methodology is also possible to obtain a complete description of the evolution of all the other parameters that characterise the debris cloud.

When the meteoroid enters the atmosphere, it is modelled using the two-dimensional single body dynamics (Sec.3.1) until the breakup. This event is triggered when the dynamic pressure at the stagnation point of the object reaches the meteoroid strength limit (S) and it is assumed instantaneous [10,37].

$$S = \rho\, v^2 \tag{27}$$

where ρ is the air density and v the meteoroid velocity at the breakup.

Moreover, it is assumed that after the entire meteoroid undergoes fragmentation, no other breakup events will occur.

At the breakup point a cloud of fragment is generated using the ABM (Sec. 2). The fragmentation model requires the definition of the range of fragments size considered. There is not a fixed rule for defining the characteristic length boundaries; they must be selected depending on the data available and of the analysis objective. In this paper, for a comparative analysis with a MC approach, it is suggested to consider fragments ranging from $L_c = 0.1\ m$ to the 70% of the meteoroid diameter at breakup.

Once the samples have been generated from the joint PDF (Sec. 2.6), the cloud density evolution is then simulated exploiting the continuity equation coupled with the dynamics (23) until they reach the ground. The integration is stopped in advance if the fragments either ablate or reach a negligible level of kinetic energy (15 J).

Considering the typical entry meteoroid scenario (described in detail in Sec. 5): very high entry velocity and relatively steep flight path angle, together with the distributions chosen in the ABM, the sampling of the joint PDF generates a "columnar shape" domain. The joint PDF is a five-dimension function, but in this section a reduced sampling of the three most relevant states is been consider for clarity: the domain in $v, A/M$ and γ space is given in Fig. 5, while, in Fig. 6, the full states sampling is given using histograms along each dimension.

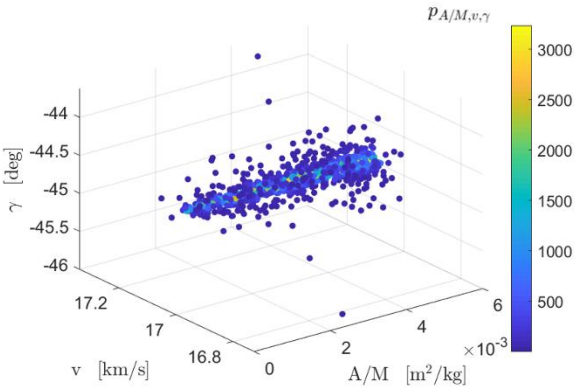

Fig. 5. Representation of a 1000 fragments sampling of the joint PDF in simplified three-dimensional phase space.

As Fig. 5 shows, the Δv generated by the ABM is not enough to create a large variation in the fragments velocity and trajectory. On the other hand, the fragmentation causes a large variation in the A/M dimension with a predominance of small fragments. As a result, the domain is elongated in A/M direction and condensed along the other states.

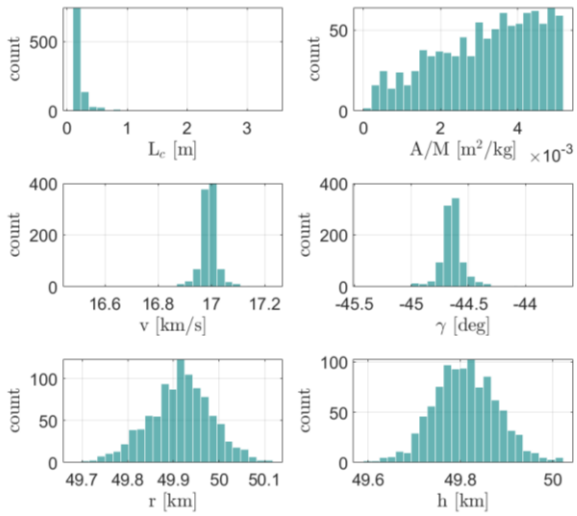

Fig. 6. Representation of a 1000 fragments sampling of the joint PDF by means of histograms in each dimension.

When evolving in time, the domain extends along the A/M dimension and shrinks in the other dimensions. As

the time passes, it progressively transforms into a line. The Fig. 7 shows this behaviour describing with differ colours the domain time evolution for the whole trajectory.

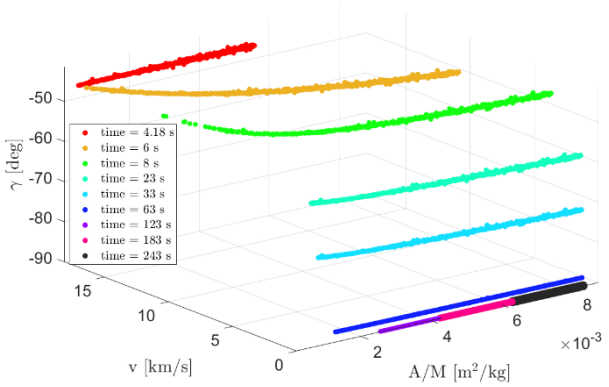

Fig. 7. Domain evolution in time

The fitting of these samples performed exploiting the Starling suite [28,35] provides good results only for the initial part of the trajectory, then some simplification are required to provide more precise results. The main criticality in the domain shape is due to the large A/M interval considered, the cause of the columnar shape. For this reason, in this paper are proposed two different strategies: reduce the A/M domain or simplify the A/M distribution.

The first method considers only the larger fragments in the distribution because they are the ones of main concern for a risk analysis. The second, exploits a binning technique for discretise the A/M dimension and makes use of the interpolation to recover the fragments distribution on the whole domain.

4.1 Reduced domain

In this simplified case, the fragment cloud fitting is performed on a reduced domain along the A/M dimension. This strategy considers only the larger fragments generated at the breakup. The reason behind this choice is to reduce the domain tendency to the elongation: the heavier objects evolve relatively slowly, hence reaching the ground before the shape of the domain becomes too complex.

The new domain evolution is presented in the Fig. 8. It can be seen that, differently from Fig. 7 the shape of the domain remains relatively confined. It should be noted that also in this case the shape of the domain is complex, the main differences from the previous case is that the range of variation of each variable is sensibly reduced, thus reducing the fitting difficulties and allowing Starling to reach good fitting results for the whole trajectory. With this strategy the joint PDF and its marginals can be available at every time step.

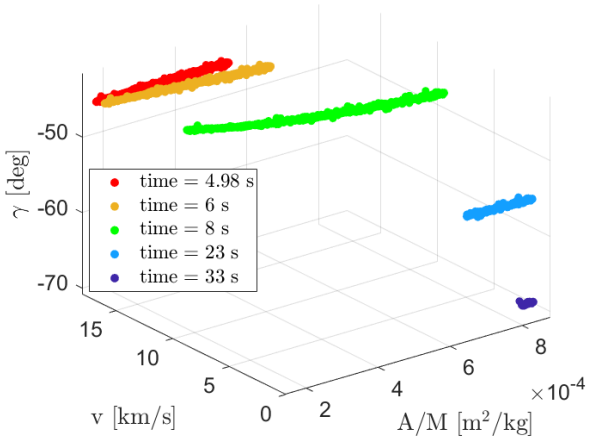

Fig. 8. Domain evolution in time considering only fragments larger than 1m in diameter.

4.2 *Area-to-Mass binning*

The binning method relies on the approximation of the A/M distribution: the PDF is approximated using a piecewise linear function. For each bin, a representative object is propagated and at the end the fitted PDF of each object are summed considering the population of each bin. This procedure is general and can be used for evaluating any states of interest, in this work the analysis is focused on evaluating the distribution of the fragments at ground. A number N_b of bins in area-to-mass ratio dimension is defined, for each bin an average A/M is assumed and the corresponding partial density is obtained according to the A/M probability density function Eq. (8). For a preliminary analysis $N_b = 10$ bins are selected and, for each one of them a representative object is chosen as the average between the bin edges:

$$A/M_{bin_i} = 1/2\ (A/M_i + A/M_{i+1}) \tag{28}$$

The probability density considered is then the probability of each A/M bin multiplied by the weight of each bin over the domain (i.e. the area associated with each bin).

$$w = \int_{A/M_i}^{A/M_{i+1}} PDF_{A/M}\, dA/M \tag{29}$$

$$PDF_{A/M_{bin_i}} = w\ PDF_{A/M}(A/M_{bin_i}) \tag{30}$$

In this way the conservation of the area under the function is guaranteed.

Different binning strategies can be adopted. After comparing different options [38], the log-spaced strategy has been chosen. Compared to a uniform binning, the log-spaced option has a denser discretisation for the lighter fragments without neglecting the heavier ones.

Fig. 9 shows the approximation of the probability density function using a piecewise linear function based on a log spaced binning.

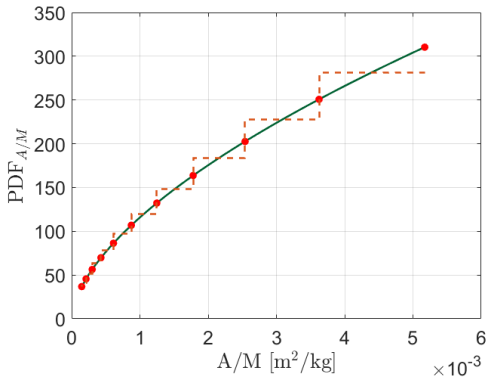

Fig. 9. PDF$_{A/M}$ approximation with a piecewise linear function (10 bins).

Each one of these bins is integrated and propagated independently from the others. For each one of them the fragments have all the same size, while the other parameters are assumed to vary following the usual ABM. Using this strategy, the evolution of the domain is greatly simplified: its shape is not elongated anymore but remains compact trough time. Fig. 10 shows the domain evolution in the reduced three-dimensional phase space considering 1-meter fragments cloud.
In this case, the Starling fitting is able to obtain good results for every bin at every time along the trajectory.

The use of the binning approximation gives on more advantage: the range distribution at the time of impact can be approximated as the range distribution at ground, in fact, since the fragments in each bin are identical and the velocity and angle variation are relatively small, the objects move close to each other along the trajectory.

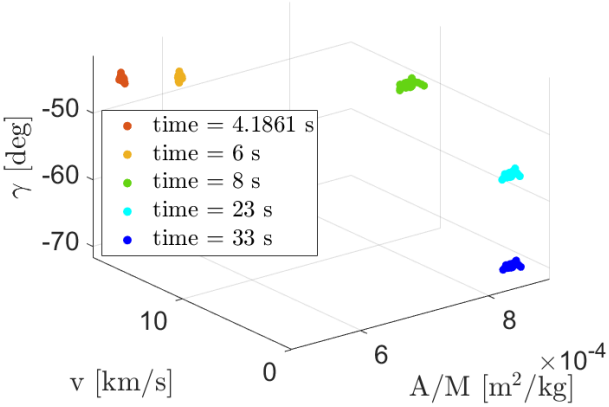

Fig. 10. Domain evolution in time considering a cloud of 1 m fragments.

As consequence, at each time the height variation between the fragments is small. This approximation is especially valid for small fragments because of the lower velocity, but it can be proved reasonable also for bigger fragments.

5. Validation

In this section, the methodology outlined in Sec. 4 is applied to recover the ground fragments distribution for a meteoroid entry event. Then the results obtained are compared with a traditional three-dimensional Monte Carlo approach. The test case selected has been obtained considering average parameters among the past meteoroid impacts.

Analysing the falls reports, the most common meteorites recorded are ordinary chondrites, hence belonging to the L class [39]. The selected diameter is 5 m: bigger objects are less frequent and there is a chance for them of having a rubble pile structure, which is less consistent with the proposed approach as it is based on the assumption of homogeneous meteoroids. Smaller bodies, instead, could have a higher strength that prevents the explosive fragmentation. The entry altitude is considered at the Karman line (formal boundary between Earth's atmosphere and outer space), while the entry velocity is taken as an average of many meteoroid entry records [40]. The flight path angle is assumed to be 45 degrees, which is considered the most probable entry angle by Shuvalov [41]. Starting from the meteoroid size and class, the meteoroid density and all the relevant parameters are inferred as explained by Cotto-Figueroa [14]. Table 1 summarises the selected meteoroid parameters and all the initial parameters assumed for the atmospheric entry.

Table 1. Hypothetical entry scenario initial parameters and meteorite characteristics.

Initial Parameter	Value
Meteoroid Class	L
Density (ρ_m)	2900 kg/m^3
Diameter (L_c)	5 m
Mass (M)	189.80 tons
Strength (S)	10^6 Pa
Ablation Coeff. (c_a)	10^{-8} s/m^2
Drag Coeff. (c_d)	1
Velocity (v)	17 km/s
Flight Path Angle (γ)	$-45°$
Altitude (h)	100 km
Longitude (λ)	0°
Latitude (δ)	0°

5.1 Strewn Field – Reduced domain approximation

The strewn field is represented by the fragments range distribution at ground. However, the range

marginal available from the PDF fitting are referred to fragments sampled at a fixed time.

Considering a fitting at a time t, the joint PDF and its marginals are available. The altitude marginal (m_h) is the probability of the fragments to be at a certain altitude at the time t, while the two-dimensional marginal of range and altitude ($m_{r,h}$) represents the probability of a fragment to be located in a particular position on the trajectory plane at the time t. The probability of having a certain range at ground (zero altitude) is then given by:

$$m_{r|h=0} = \frac{m_{r,h}}{m_h} \tag{31}$$

For each snapshot, in which the fragments reach the ground, the marginals have been computed and transformed. To obtain the global range PDF, the marginals are summed and weighted with the normalised number of fragments that reach the ground at every time step as follows:

$$PDF_{range} = \sum_{i=T_0}^{T_f} w_i \, m_{r|h=0_i} \tag{32}$$

where T_0 and T_f represents the boundary of the time window in which the snapshots have been considered, and w_i is the weight (normalised number of fragments at ground) of each snapshot.

At this point, as outlined in Sec 3.4, the range can be decomposed, by means of the χ distribution in the δ and λ angular range. Then, the distribution is written in terms of the ground coordinates X and Y, obtained by multiplying latitude and longitude by the Earth radius.

$$p_{X,Y} = \frac{m_r \; p_\chi}{R_E} \tag{33}$$

For the case analysed, the falling fragments time windows goes from $t = 9\,\mathrm{s}$ to $t = 36\,\mathrm{s}$. The time discretisation chosen is of $1\,s$. The following figures represent the PDF at ground obtained with the density-based approach (Fig. 11) and the comparison with a Monte Carlo simulation (Fig. 12).

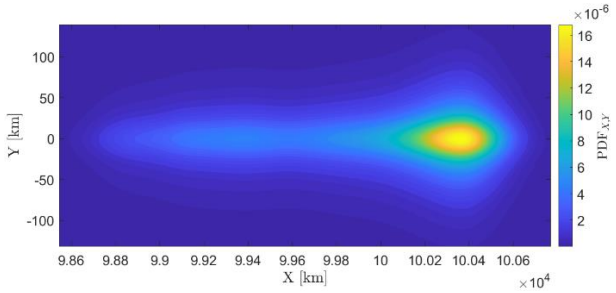

Fig. 11. Strewn field distribution obtained using the density-based methodology.

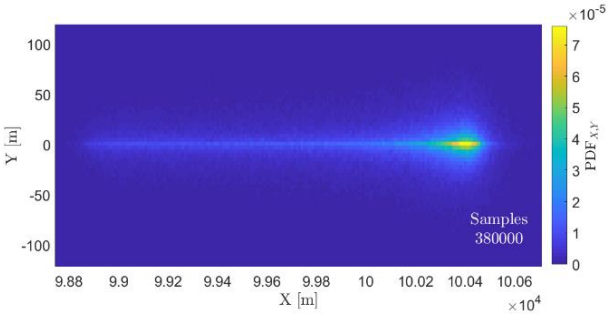

Fig. 12. Strewn field distribution obtained using the Monte Carlo simulation.

The density-based approach provides a good estimation of the MC result. There is a small difference in the scale of the density: the MC distribution has a higher peak, then it decreases faster than the PDF found with the density-based approach. This is probably due to the approximations used in the three-dimensional methodology and to the time discretisation approximation used for estimating the joint PDF. However, it should be reminded that the MC analysis required a very high number of samples in order to estimates correctly the footprint distribution, while the methodology used in this paper is capable of reaching comparable results with only 1000 samples. The Fig. 13 represents the strewn field distribution obtained with a MC analysis that use the same number of samples adopted in the density based approach.

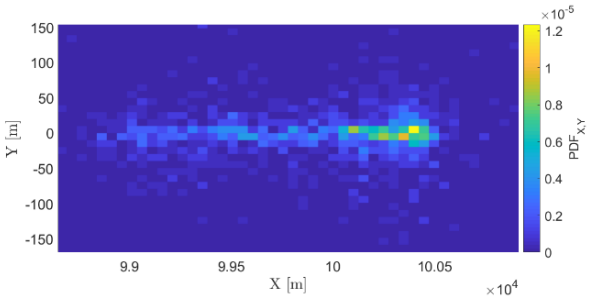

Fig. 13. Strewn field distribution obtained using the Monte Carlo simulation with 1000 samples.

5.2 Strewn Field – Binning approximation

Exploiting this strategy, the fitting provides good results for every bin at every time along the trajectory. The use of the binning approximation gives on more advantage: the range distribution at the time of impact can be approximated as the range distribution at ground. In fact, since the fragments in each bin are identical and the velocity and angle variation are relatively small, each object moves close to the others along the trajectory. As consequence, at each time the height variation is between the fragments in the cloud is small. This approximation is especially valid for small fragments because of the lower velocity.

The Fig. 14 proves the validity of this assumption showing the range probability density function fitted at the time of impact and the range distribution at ground estimated using a MC simulation for 1 meter fragments.

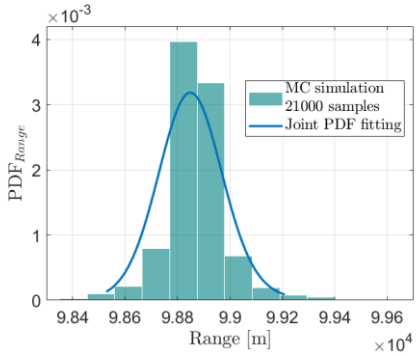

Fig. 14 Comparison in range PDF between the joint PDF fitting and MC simulation for a 1 m fragments bin.

Even if the domain remains relatively compact, when analysing the smaller fragments some problems arise in the fitting when γ approaches 90 degrees. In fact, the straight angle is the accumulation point of γ: after some time, the lighter bodies will fall vertically causing the collapsing of the flight path angle dimension. Then, all the other parameters will evolve independently from γ. This behaviour is not currently supported by the Starling software, so it should be treated with a different approach. Since this analysis focus on the range determination and when $\gamma \sim 90°$ the range can be approximated constant in time, hence, when analysing the smaller fragments, the fitting is performed slightly before the 'vertical fall' event. The smaller the fragments are, the bigger is the inaccuracy of this approximation, because they reach the limit angle at higher altitude. Then, if the trajectory is not exactly perpendicular to the ground, the range distribution evaluated at a high altitude can be different from the one at ground, causing a non-negligible variation in the footprint determination. After evaluating each marginal for each bin, the weighted sum is performed. In the test case considered, the strewn field distributions of each bin are narrow, and their summation does not give a smooth function. The results is given in the planar frame for clarity in Fig. 15.

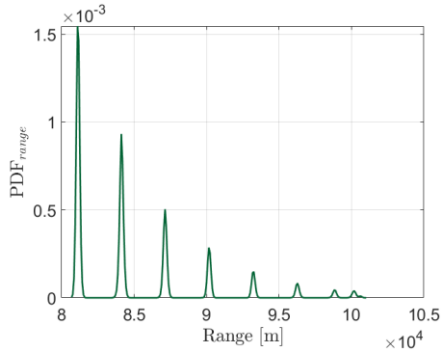

Fig. 15. Weighted sum of all the range PDFs.

The resulting total range distribution shows peaks in correspondence to each one of the selected bins. It is then considered a denser bin grid, but among the bins generated, only few of them are propagated. Then, the range PDFs obtained are approximated as points in correspondence with each maximum, since these distributions are very narrow with respect to the footprint range on ground. In this way, interpolating these points and imposing the unitary total area under the function, it is obtained a smooth function that describes the fragments density on ground. The Fig. 16 presents the new range PDFs, considering 64 bins, 10 of which have been propagated and fitted.

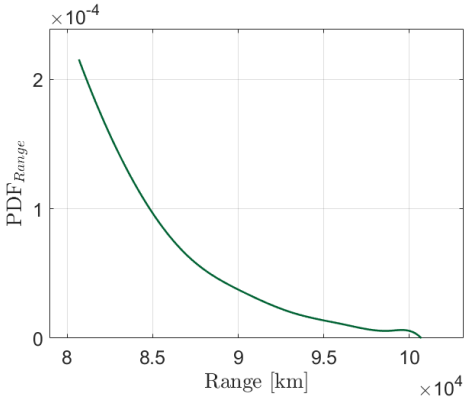

Fig. 16. Mono-dimensional strewn field distribution obtained with the binning approximation.

The peaks disappeared, and the resultant function is smooth. The function obtained agrees with the MC estimation (Fig. 17) except for in the right end part of the curve. That is probably due to the fact that the approximation of the time fitting with the altitude fitting assumed in this analysis is weaker for the big and fast fragments.

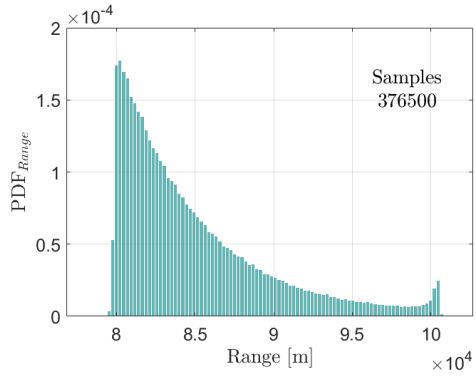

Fig. 17 Mono-dimensional strewn field distribution obtained using the Monte Carlo simulation.

This approach can be generalised also using a full state PDF. In this case it is obtained a two dimensional strewn field distribution (Fig. 18) that is compared with the traditional MC approach estimation in Fig. 19.

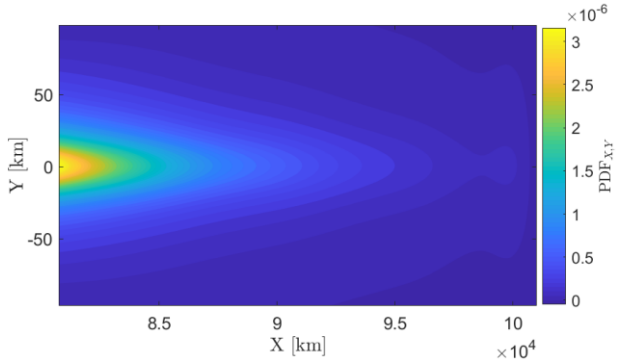

Fig. 18. Strewn field distribution obtained using the density-based methodology.

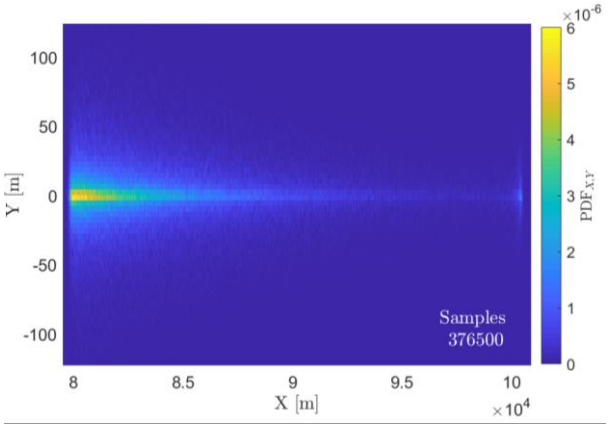

Fig. 19. Strewn field distribution obtained using the Monte Carlo simulation.

The strewn field obtained with the density-based approach is comparable with the one obtained from the MC estimation. The values estimates with the MC simulation is higher, that means that the fitting of the density function overestimate the spreading of the fragments around the symmetry axis, this is probably an effect of the approximation of the χ angle constant and independent of the others states. It should be noted that also the peak of the right end part of the MC simulation has been represented by the fitting, even if its associated probability is lower with respect to the one in the MC. As in its two-dimension counterpart, also in this case the density-based result, lack of a representation of the function behind the peak.

5.3 *Fragments size distribution at ground*

Another variable of interest used for characterising the strewn field is the fragments size distribution (A/M) inside the footprint area. This kind of analysis is particularly useful because it relates the position, the size and the frequency of the fragments at ground.

The binning methodology presented previously is used for evaluating the PDF marginal in a two-dimensional phase space. In particular, the fragment probability density function is considered along the range (i.e. the distance travelled along the orbit ground track) and A/M dimensions. In this way, a complete description of the strewn field could be achieved.

In order to obtain a map of the A/M fragments distribution along the strewn field axis the same passages described in Sec.5.2 has been exploited. The distribution obtained is a curved bi-dimensional plane (Fig. 20) in agreement with the ones estimated with a MC simulation (Fig. 21). The smaller fragments have a large probability density value and are located at the leading edge of the strewn field (i.e. small range distance). The density value decreases progressively as the range increases so that at the opposite side of the strewn field are located the bigger fragments.

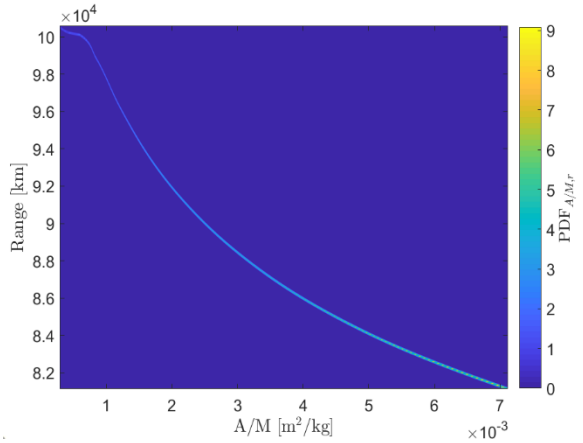

Fig. 20. Fragments distribution field obtained using the density-based methodology.

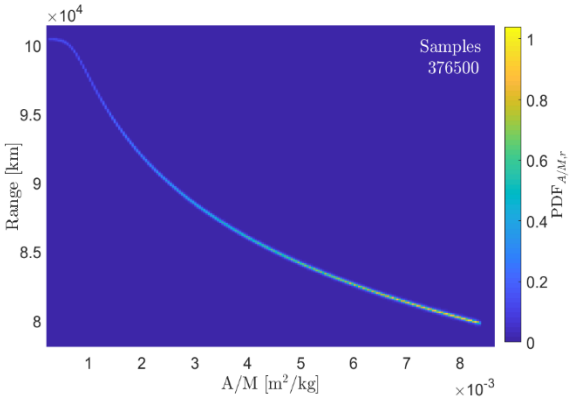

Fig. 21. Fragments distribution obtained using the Monte Carlo simulation.

Similarly, to the strewn field distribution, the two representations obtained are similar and differ slightly only on the density magnitude. This behaviour is likely due to the binning approximation used to have a better-behaved domain on which perform the fitting.

6. Real case application

The methodology, validated in Sec. 5, is now applied to the analysis of a real entry scenario: the 2008TC$_3$ fall

[42–44]. 2008TC_3 is an asteroid similar in size to the hypothetical one used to validate the model. The purpose of this analysis is to highlight the differences between a real case scenario and a simulated one. From their comparison, we can understand the limitations of the model and deduce gain insight for future developments. Thanks to the high quality of the available data, the analysis of the 2008TC_3 fall provides strong and unique observational constraints to test the accuracy of the models used for strewn filed determination.

The asteroid 2008 TC_3 was observed on October 6, 2008 and the impact occurred above the Nubian Desert in northern Sudan [44]. The entry velocity relative to the ground was 12 km/s with an γ of 21 degrees [42]. Jenniskens [43] found that the asteroid broke up at an altitude of 37 km. Over 600 meteorites were recovered from the impact site, most of them of small dimension, with a total mass of 10.7 kg [44]. The subsequent analysis of the meteorites indicated that the asteroid was an achondrite and that its original diameter was about 4 m.

Table 2 summarises the parameters of the meteoroid at the entry that have been used in the simulation. However, some of the data required were not directly available from literature reports. For example, the ablation coefficient and the strength of the meteoroid. In these case reasonable assumptions have been made starting from the information available. Regarding the strength, knowing the altitude of fragmentation, it can be reasonably estimated computing the dynamic pressure at that altitude. On the other hand, a direct estimation of the ablation coefficient is not possible from the data available, hence the same value used in Section 5 has been adopted (Table 1).

Table 2. 2008 TC_3 meteorite characteristics and re-entry initial conditions.

Initial Parameter	Value
Meteoroid Class	Urelite
Density (ρ_m)	2800 kg/m^3
Diameter (L_c)	4 m
Mass (M)	94 $tons$
Strength (S)	2.2 10^6 Pa
Ablation Coeff. (c_a)	10^{-8} s/m^2
Drag Coeff. (c_d)	1.8
Velocity (v)	12.38 km/s
Flight Path Angle (γ)	$-21°$
Altitude (h)	100 km
Longitude (λ)	30.54°
Latitude (δ)	21.09°

It is also important to point out that the drag model used is not an accurate representation of the behaviour of 2008 TC_3 in the atmosphere. The asteroid experienced different drag coefficient depending on its orientation, but the constant value of c_d = 1.8 could represent a good approximation as Farnocchia et al. [42] pointed out. On more remark is needed on the fragmentation phenomenon: in this simulation the fragmentation is treated as a unique event, but as Jenniskens et al. [43] observed, the asteroid showed significant disruption at altitudes around 42, 37 and 33 km. However, the methodology described in this paper currently do not support multiple fragmentation point along the trajectory. For this reason, in the simulation the altitude selected for the fragmentation is 37 km and it is assumed that all the fragments are generated at that instant. This assumption must be taken into consideration when comparing the results of the simulation with the real data.

6.1 Strewn field

Fig. 22 shows the ground-projected approach path of the asteroid over the Earth Surface and the location of the fragments collected after the impact. The masses recovered range from 1.5 g to 283 g spreads for 29km along the approach path. To analyse this scenario, it has been exploited the binning strategy (Sec. 5.2) for the domain fitting. This was judged the most reliable strategy because it is the only solution scheme that correctly estimates the smaller fragments distribution. Moreover, considering that only small meteorites have been recovered in this strewn field (Fig. 22) this approach was judged more solid.

As explained in Sec. 3 the ABM requires as input, together with the states of the asteroid at the breakup, also the maximum and minimum fragments size produced at breakup. Differently from the Sec. 5, in which the size of fragments produced by the ABM are assumed to be between 0.1 m and the 70% of L_c at the breakup, in this analysis these boundaries have been modified. In fact, the fragments recovered from the meteoroid impact are much smaller than the original size of the body. The smaller fragments size at breakup is assumed to be 5 cm, while the maximum limit is assumed to be 1 m.

Fig. 23 represents the normalised fragment density on ground: the yellow regions is the one with more concentration of fragments, while the blue region represents the absence of objects. Comparing the strewn field resulted from the simulation with the real one, it is possible to observe some differences, but also some similarities. First of all, the location of the strewn field on the Earth surface is reasonably estimated by the model, despite the assumptions made (i.e. non-rotating Earth, constant drag coefficient, constant heading angle, etc.). The comparison shows a good accuracy of the latitude together with a small drift of the longitude towards west. Globally this proves that the model can reasonably estimate the location of the strewn field. However, the shape of the footprint has relevant differences: the simulation shape can be approximated as a line, while in the real case, even if it is possible to identify a line that

interpolates the fragments location, the fragments are more spread.

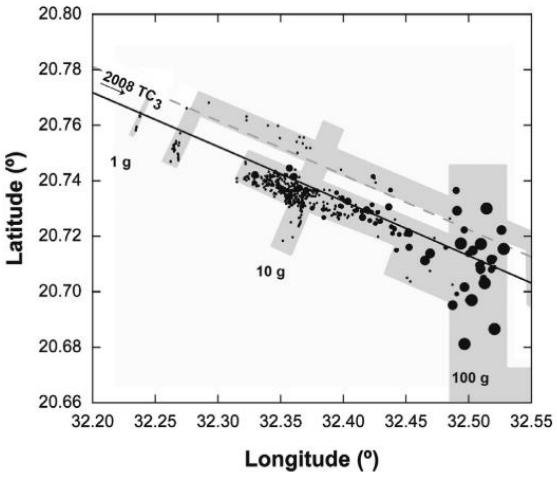

Fig. 22. Drag-free ground track (solid line) and meteorite locations (black dots). Larger dots correspond to larger meteorite sizes. In grey, the area explored by Jenniskens [43] and Shaddad et al. [43]. The dashed line is the ground track used by Jenniskens, while the black ones is the one used by Farnocchia et al. [42] that include Earth's J2.

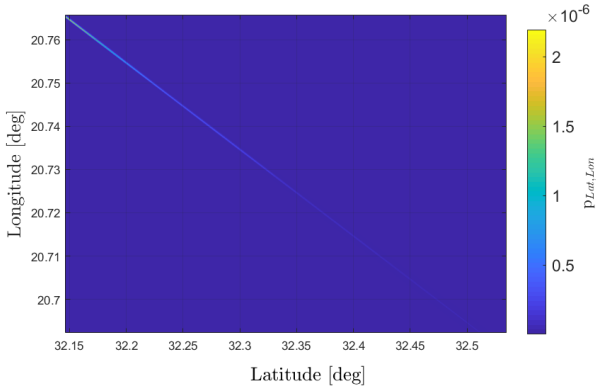

Fig. 23. Strewn field shape obtained from the simulation. The probability values represent the normalised fragments density

Moreover, while in the model the line gets narrower as the strewn field evolves toward the left, in the real case the strewn field shows the opposite behaviour (Fig. 23). This behaviour is different also from the typical shapes on the asteroids strewn field, for which the bigger fragments tends to be aligned with the ground track of the asteroid [33]. The difference between the model and the real footprint could be caused both by the Δv distribution used in the ABM (that has not been modified from the original one in the NASA SBM) and also to the one fragmentation point approximation. In fact, multiple breakups can contribute to increasing the fragments spread (i.e. the velocity of each fragment is scattered multiple times).

Another features to highlight in the real strewn field is that the smaller fragments show a south offset with respect to the ground track, which is likely caused by winds at the time of the atmospheric entry. Winds and side forces have not been considered in the model proposed, so this could have been another source of inaccuracy. Despite of that, the model correctly estimates the fragments density along the ground track: there is an higher density of fragments at the start of the strewn field (left part of the figure), that diminish going towards the right part of the figure. This behaviour seems different looking at the real strewn field, but it should be noticed that the meteorites have been searched only on the grey rectangles area. Furthermore, it is difficult to identify meteorites fragments too small. For these reasons it is reasonable to assume that in the left part of the figures more fragments exist, but they have not been found yet. It could also be possible that the smaller fragments would have dispersed by the cross winds, like dust.

6.2 Fragment distribution

The Fig. 23 is incomplete: it gives information only on the fragment density, but no information on their size. For this reason, for a more comprehensive analysis it should be coupled with Fig. 24, that represents the fragments A/M distribution in function of the latitude distance. It shows that the smaller fragments are more and are concentrated at smaller longitude, while the bigger fragments are rare and concentrated at higher longitude, coherently with what is observed in the real strewn field.

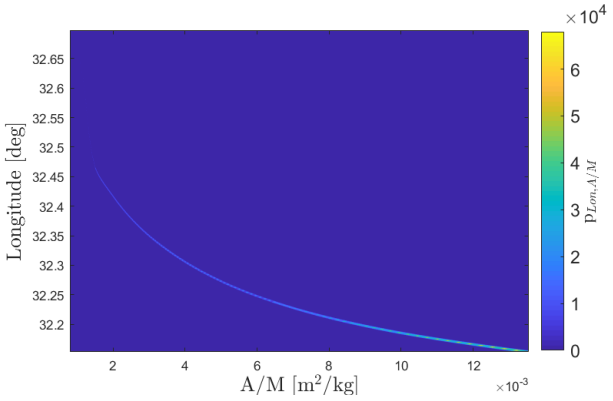

Fig. 24. A/M distribution along the latitude obtained from the simulation.

There is a substantial difference with respect to the real fragments' location: the A/M range of the simulation is considerably bigger than the one of the observed footprint. An A/M value of 12 10^{-3} m^2/kg corresponds to 130 g, while 2 10^{-3} m^2/kg corresponds to 28 kg. The presence of the big masses larger than the meteorites collected on ground, in the simulated strewn field is due to the limits imposed on the size using the fragmentation

model. A bound lower than 1 m where judged infeasible for a fragmentation of a 4 m-asteroid. However, it should be reminded that the proposed methodology is based on a probabilistic model: the absence of big fragments on the real case is compatible with the low probability density value estimated with the continuum approach. However, an overestimation of kilograms sizes fragments could derive from the model uncertainty (i.e. multiple fragmentation points or σ_{ab} overstimation). In Fig. 24, the objects of different sizes are more grouped with respect to the real footprint, also in the along-track direction. In fact, the masses below 130 grams are located before the 32.2° of longitude, while in the real strewn field, in the same area only the masses of 1 gram are found. Similarly, as the lack of spread in the direction perpendicular to the along track direction highlighted previously, this behaviour could be probably due to the underestimation of the Δv at the breakup or to the multiple fragmentation points experienced in the real case.

7. Conclusions and future work

The aim of this paper was to investigate the phenomena experienced by big meteoroid and small asteroid during the atmospheric entry. Among these, specific attention has been dedicated to the fragmentation phenomenon and to the subsequent evolution of the cloud of fragments towards the ground.

A novel approach to the meteoroid fragmentation modelling has been proposed that can provide an estimation of the parameters of all the fragments generated at breakup. This model describes the fragments cloud by means of a continuous distribution function defined in the *A/M*, *v*, γ space. To take advantage of the continuum formulation of the fragments cloud, a density-based methodology has been exploited for the dynamics propagation.

The meteoroid fragments during the re-entry generate a peculiar domain, characterised by an elongated shape, that evolves quickly in time and that it is difficult to fit accurately. Simplifying the domain or analysing only the larger fragments have been proven feasible strategies that gives good predictions for the fragments strewn filed, comparable to a Monte Carlo simulation. This result is of particular relevance, because the main drawback of the Monte Carlo simulations is the high number of sampling required to provide a good estimate of the distributions. The density-based methodology, instead, reached the same results with only a limited number of samples.

In the last part of the paper is analysed the $2008TC_3$ impact. The results obtained showed a good approximation of the landing site. However, differently form the real strewn field, the one resulted from the simulation is narrower both in the along-track dimension and in the perpendicular one. Furthermore, the location of fragments inside the strewn field obtained does not match accurately the one recorded on ground. This reduced accuracy could be caused either from the ABM, that underestimate the velocity difference between the fragments after the breakup, or from the approximation used for the dynamic model that does not account for the Earth's rotation, the presence of crosswinds and the occurrence of multiple breakup. Probably each one of the previous points contributes in part to the differences between the two strewn filed.

Further investigation is needed to assert the quality of the results of the ABM: the direct extension of the NASA SBM to asteroids fragmentations should be further refined including experimental data, for a better use in real applications. Regarding the dynamics propagation, further analysis on the meteorites or dedicated mission on asteroids could help to have a better understanding and estimation on the asteroids physical properties. Starting from that, more accurate ablation and drag models could be produced and implemented in the model.

Furthermore, in some cases the fragments generated experienced further fragmentations during the descent. The model used in this work assumes only one breakup point along the meteoroid trajectory. A further possible development could take into account the presence of multiple fragmentation points or, similarly, this model could also be integrated in others existing parent-child models in order to permit a more detailed representation of the cloud of the small fragments.

It should be highlight that the structure of the methodology presented in this thesis permits to integrate eventual more refined fragmentation models, when available, without any modification on its other parts.

Acknowledgements

This project has received funding from the European Research Council (ERC) under the European Union's Horizon 2020 research and innovation programme (grant agreement No 679086 - COMPASS). The authors would like to thank Alberto Buzzoni, Senior Associate Astronomer of the National Institute for Astrophysics and Daniele Gardiol, Primo Tecnologo at the National Institute for Astrophysics- Osservatorio Astrofisico di Torino for the their suggestion on the real scenarios used for this paper.

Appendix A (Probability density function transformation)

By definition a given probability density function, $p_x = p(x)$ that by definition is required to sum to unity if integrated over the whole state space x.

The fragment distribution, instead, is described by the phase space density n_x, that is the number of fragments in an infinitesimal volume around a state x. The integration of it over the full domain yields the total number of fragments, N.

$$\int_{-\infty}^{+\infty} n_x \, dx = N \tag{34}$$

Since n_x and the p_x only differ via the normalization constant, the space density function can be treated as a probability density function.

At this point, considering a one-to-one change of variables, $y = \boldsymbol{\varphi}(\boldsymbol{x})$ with $\boldsymbol{x}, \boldsymbol{y} \in \mathbb{R}^n$. If $\boldsymbol{\varphi}$ is differentiable, then the probability density function p_y can be derived from the probability density function p_x in the following way [45]:

$$p_y(\boldsymbol{y}) = \frac{p_x(\boldsymbol{\varphi}^{-1}(\boldsymbol{y}))}{|det \boldsymbol{J}|} \tag{35}$$

With the Jacobian $\boldsymbol{J} \in \mathbb{R}^{n \times n}$ defined as

$$J_{i,j} = \frac{\partial \varphi_i}{\partial x_i} \tag{36}$$

If the function $\boldsymbol{\varphi}$ is not invertible, the probability then is the sum of all the possible inputs [46].

References

[1] Q.R. Passey, H.J. Melosh, Effects of atmospheric breakup on crater field formation, Icarus. 42 (1980) 211–233. https://doi.org/10.1016/0019-1035(80)90072-X.

[2] O.P. Popova, P. Jenniskens, et al., Chelyabinsk airburst, damage assessment, meteorite recovery, and characterization, Science (80-.). 342 (2013) 1069–1073. https://doi.org/10.1126/science.1242642.

[3] J.G. Hills, M.P. Goda, The Fragmentation of small Asteroids in the atmosphere, Astron. J. (1993).

[4] D.O. ReVelle, NEO fireball diversity: Energetics-based entry modeling and analysis techniques, Proc. Int. Astron. Union. 2 (2006) 95–106. https://doi.org/10.1017/S1743921307003122.

[5] Z. Ceplecha, D.O. ReVelle, Fragmentation model of meteoroid motion, mass loss, and radiation in the atmosphere, Meteorit. Planet. Sci. 40 (2005) 35–54. https://doi.org/10.1111/j.1945-5100.2005.tb00363.x.

[6] N.A. Artemieva, V. V. Shuvalov, Motion of a fragmented meteoroid through the planetary atmosphere, J. Geophys. Res. E Planets. 106 (2001) 3297–3309. https://doi.org/10.1029/2000JE001264.

[7] P.M. Mehta, E. Minisci, et al., Break-up modelling and trajectory simulation under uncertainty for asteroids, Proceeding 4th IAA Planet. Def. Conf. Frascati, Roma. (2015) 13–17.

[8] V.A. Andrushchenko, N.G. Syzranova, Mathematical Simulation of the Fall and Fragmentation of the Sikhote-Alin Bolide, Math. Model. Comput. Simulations. 11 (2019) 451–456. https://doi.org/10.1134/S2070048219030037.

[9] L.F. Wheeler, P.J. Register, et al., A fragment-cloud model for asteroid breakup and atmospheric energy deposition, Icarus. 295 (2017) 149–169. https://doi.org/10.1016/j.icarus.2017.02.011.

[10] P.J. Register, D.L. Mathias, et al., Asteroid fragmentation approaches for modeling atmospheric energy deposition, Icarus. 284 (2017) 157–166. https://doi.org/10.1016/j.icarus.2016.11.020.

[11] P.J. Register, M.J. Aftosmis, et al., Interactions between asteroid fragments during atmospheric entry, Icarus. 337 (2020) 113468. https://doi.org/10.1016/j.icarus.2019.113468.

[12] E.J. Öpik, Physics of Meteor Flight in the Atmosphere, 1959. https://doi.org/10.1063/1.3060580.

[13] D.O. ReVelle, Recent Advances in Bolide Entry Modeling: A Bolide Potpourri, 2006. https://doi.org/10.1007/s11038-005-9064-4.

[14] D. Cotto-Figueroa, E. Asphaug, et al., Scale-dependent measurements of meteorite strength: Implications for asteroid fragmentation, Icarus. 277 (2016) 73–77.

[15] E.L. Newland, G.S. Collins, et al., Meteoroid fragmentation in the martian atmosphere and the formation of crater clusters, in: 50th Lunar Planet. Sci. Conf., 2019.

[16] Z. Ceplecha, J. Borovička, et al., Meteor phenomena and bodies, Space Sci. Rev. 84 (1998) 327–471. https://doi.org/10.1023/A:1005069928850.

[17] J. Gelhaus, C. Kebschull, et al., DRAMA Final Report, 2014.

[18] R. Kanzler, T. Lips, Upgrade of DRAMA's Spacecraft Entry Survival Analysis Codes -Final Report, 2018. https://doi.org/10.2307/2608048.

[19] P.H. Krisko, Proper Implementation of the 1998 NASA Breakup Model, Orbital Debris Q. News. 15 (2011) 5.

[20] N.L. Johnson, P.H. Krisko, et al., NASA's new breakup model of EVOLVE 4.0, Adv. Sp. Res. 28 (2001) 1377–1384.

[21] D.L. Turcotte, Fractals and fragmentation, New York. 91 (1986) 1921–1926.

[22] D.D. Badyukov, A.E. Dudorov, Fragments of the Chelyabinsk meteorite shower: Distribution of masses and sizes and constraints on the mass of the largest fragment, Geochemistry Int. 51 (2013) 583–586..

[23] M. Fries, L. Le Corre, et al., Detection and rapid

recovery of the Sutter's Mill meteorite fall as a model for future recoveries worldwide, Meteorit. Planet. Sci. 49 (2014) 1989–1996. https://doi.org/10.1111/maps.12249.

[24] A. Bade, A.A. Jackson, et al., Breakup model update at nasa/jsc, Sci. Technol. Ser. (2000) 125–138.

[25] S. Frey, C. Colombo, Transformation of satellite breakup distribution from Cartesian coordinates to orbital elements, 10 (n.d.).

[26] W.B. Heard, Dispersion of ensembles of non-interacting particles, Astrophys. Space Sci. (1976). https://doi.org/10.1007/BF00640556.

[27] C.R. McInnes, Simple analytic model of the long-term evolution of nanosatellite constellations, J. Guid. Control. Dyn. (2000). https://doi.org/10.2514/2.4527.

[28] S. Frey, C. Colombo, et al., Application of density-based propagation to fragment clouds using the Starling suite, in: First Int. Orbital Debris Conf., 2019.

[29] L. Francesca, Space debris cloud evolution in Low Earth Orbit, Univerity of Southampton, 2016.

[30] M. Trisolini, C. Colombo, A density-based approach to the propagation of re-entry uncertainties, Adv. Astronaut. Sci. 168 (2019) 2241–2253.

[31] M. Trisolini, C. Colombo, Modeling re-entry break-up uncertainties with continuity equation and Gaussian mixture models interpolation, in: Proc. 2020 AAS/AIAA Astrodyn. Spec. Conf., Lake Tahoe, USA, 2020: p. AAS 20-636.

[32] A. Halder, R. Bhattacharya, Dispersion analysis in hypersonic flight during planetary entry using stochastic liouville equation, J. Guid. Control. Dyn. 34 (2011) 459–474. https://doi.org/10.2514/1.51196.

[33] O.R. Norton, Field guide to meteors and meteorites, 2009. https://doi.org/10.5860/choice.46-2639.

[34] V. a. Bronshten, Physics of Meteoric Phenomena, 1983. https://doi.org/10.1007/978-94-009-7222-3.

[35] S. Frey, C. Colombo, et al., Interpolation and integration of phase space density for estimation of fragmentation cloud distribution, in: Adv. Astronaut. Sci., 2019.

[36] G. Avanzini, Entry, Descent, Landing and Ascent Lecture notes-Ver. 1.0.3, (2009).

[37] P.M. Mehta, M. Kubicek, et al., Surrogate model for probabilistic modeling of atmospheric entry for small NEO's, in: Adv. Astronaut. Sci., 2016: pp. 1807–1822.

[38] S. Limonta, Meteoroids and Asteroids : a Density Based Approach for Entry , Fragmentation and Descent Through the Atmosphere, Politecnico di Milano, 2020.

[39] B. Carry, Density of asteroids, Planet. Space Sci. 73 (2012) 98–118. https://doi.org/10.1016/j.pss.2012.03.009.

[40] P. Brown, P.J.A. Mccausland, et al., The fall of the Grimsby meteorite-I: Fireball dynamics and orbit from radar, video, and infrasound records, Meteorit. Planet. Sci. (2011).

[41] V. V Shuvalov, N.A. Artemieva, Numerical modeling of Tunguska-like impacts, 50 (2002) 181–192.

[42] D. Farnocchia, P. Jenniskens, et al., The impact trajectory of asteroid 2008 TC3, Icarus. 294 (2017) 218–226. https://doi.org/10.1016/j.icarus.2017.03.007.

[43] P. Jenniskens, M.H. Shaddad, et al., The impact and recovery of asteroid 2008 TC3, Nature. 458 (2009) 485–488. https://doi.org/10.1038/nature07920.

[44] M.H. Shaddad, P. Jenniskens, et al., The recovery of asteroid 2008 TC3, Meteorit. Planet. Sci. 45 (2010) 1557–1589. https://doi.org/10.1111/j.1945-5100.2010.01116.x.

[45] S. Ghahramani, Fundamentals of Probability, 2015. https://doi.org/10.1201/b19602.

[46] S. Frey, C. Colombo, Transformation of satellite breakup distribution for probabilistic orbital collision hazard analysis, J. Guid. Control. Dyn. (2020).